Journal of
Mechanics of
Materials and Structures

THEORETICAL AND EXPERIMENTAL STUDIES OF BEAM BIMORPH PIEZOELECTRIC POWER HARVESTERS

Shudong Yu, Siyuan He and Wen Li

Volume 5, No. 3 March 2010

mathematical sciences publishers

JOURNAL OF MECHANICS OF MATERIALS AND STRUCTURES
Vol. 5, No. 3, 2010

THEORETICAL AND EXPERIMENTAL STUDIES OF BEAM BIMORPH PIEZOELECTRIC POWER HARVESTERS

SHUDONG YU, SIYUAN HE AND WEN LI

This paper presents a theoretical model for simulating a piezoelectric beam bimorph power harvester consisting of a laminated piezoelectric beam, a proof mass, and an electrical load. The vertical offset of the proof mass center from the beam centroid couples the bending and longitudinal motions, which makes it necessary to consider both longitudinal and lateral vibrations simultaneously. Experiments were carried out on a beam bimorph prototype mounted on a shaker to measure the electrical output. Numerical results obtained using the proposed procedure for piezoelectric bimorph power harvesters are in good agreement with the experimental data.

1. Introduction

Power harvesting devices scavenge energy from ambient mechanical vibrations. When a cantilever bimorph piezoelectric beam is attached to a vibrating base, electrical energy is produced continuously. Devices of this kind are often used to replace or extend the life time of electrochemical batteries for wireless sensors, implanted medical devices, handheld electronic devices, and other portable electronic devices [Roundy et al. 2004; Yang 2006; Liao and Sodano 2008]. Compared with other energy scavenging methods such as electromagnetic [Glynne-Jones et al. 2004] and electrostatic methods [Mitcheson et al. 2004], piezoelectric vibration based energy harvesting systems have been attracting a lot of attention recently because of their simple structure, direct conversion of vibration energy into electrical energy with a high voltage level, lower number of additional electrical components, and not requiring an electric power source [Sodano et al. 2004; Anton and Sodano 2007]. The most popular structures for vibration based piezoelectric power harvesting systems are piezoelectric cantilever (unimorph or bimorph) beams, which are suitable for small amplitude ambient vibration. Most test results available in the literature were obtained for sinusoidal mechanical motion. Cantilever-type energy harvesting devices function most effectively when the excitation frequencies vary in the vicinity of the fundamental resonant frequency of the electromechanical system.

Models of distributed-parameter energy harvesting systems were presented in [Erturk and Inman 2008b], and approaches based on modal analysis were proposed to solve the dynamical response of the electromechanical system. An energy-based formulation of piezoelectric structures is given in [Dutoit et al. 2005]. Some simplified analytical models for a cantilever piezoelectric beam energy harvester are available in the literature. However, as pointed out in [Erturk and Inman 2008a], errors were unfortunately present in deriving the simplified analytical solutions in several published papers. The authors of the current paper also had the opportunity to examine the analytical results published in the literature, and observed that errors and mistakes of a nontypographical nature indeed existed in the earlier works

Keywords: power harvesting, finite element modeling, piezoelectric structures, bending, axial deformation, rotary inertia.

concerning the derivations of analytical solutions for bimorph piezoelectric structures. The timely paper [Erturk and Inman 2009] deals with the analytical solution for a bimorph piezoelectric beam energy harvester carrying a symmetrically placed proof mass.

In this paper, the finite element method is employed to obtain the governing equations of the electromechanical system consisting of a piezoelectric beam, a proof mass, and a resistive load. The three-node beam element [Yu and Cleghorn 2002], presented in this paper, is of a higher order type and is ideal for dynamic problems. The authors anticipate that energy harvesting devices of this type can be modeled accurately using the proposed method. Effects of mass, mass moment of inertia, and offsets of the mass center with respect to the mass-beam interface can be studied for a proof mass of general configuration.

2. Formulation of mechanical and electrical energies

A piezoelectric power harvester consisting of a piezoelectric bimorph beam and a proof mass is sketched in Figure 1. The piezoelectric beam is clamped onto a vibrating base. As the base vibrates, the mechanical energy is converted into electrical energy through the piezoelectric power harvester. In this section, the mechanical (kinetic, strain, and dissipative) energy, the electrical energy, and the electrical work done on a power-consuming resistor are studied and related to a set of electromechanical variables.

Axial strain. The axial strain everywhere in the piezoelectric beam is induced by the axial and lateral deformations in the x-z coordinate plane (see Figure 1). Within the context of classical beam theory, a plane of a beam normal to its neutral axis before deformation remains a plane and normal to the deformed neutral axis after deformation. The total axial displacement of a material point in the beam structure,

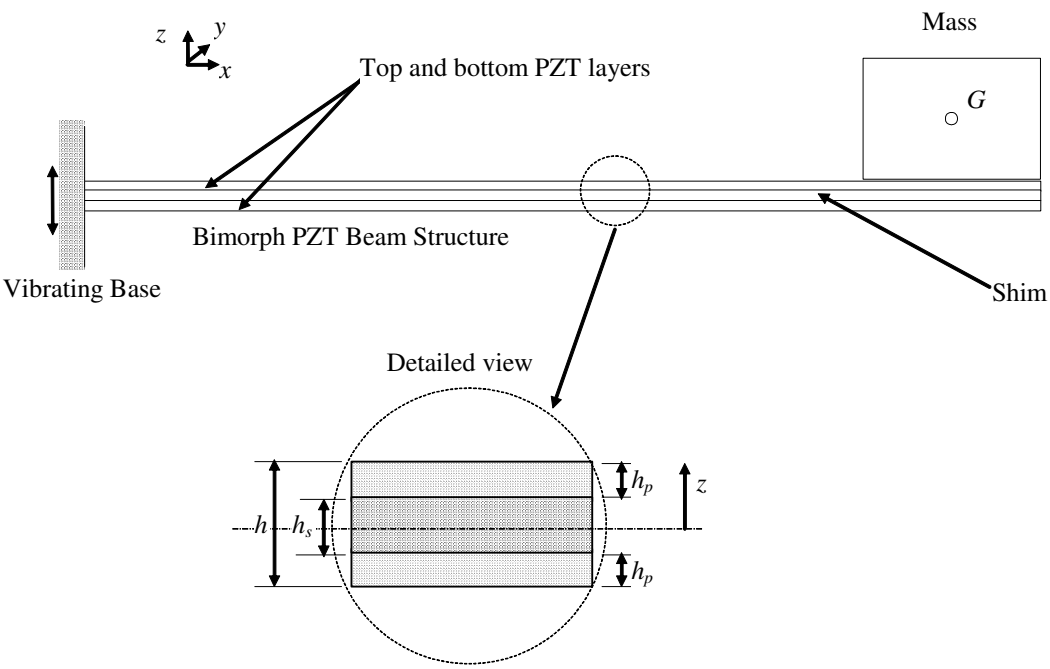

Figure 1. Illustration of a typical piezoelectric power generator.

bounded by $0 \le x \le l$, $-b/2 \le y \le b/2$, and $-h/2 \le z \le h/2$, may be written as

$$u(x, z, t) = u_0(x, t) - \theta(x, t)z, \tag{1}$$

where $u_0(x, t)$ is the axial displacement due to uniform axial stretching, $w(x, t)$ is the lateral displacement of the centroid due to in-plane bending, z is the vertical distance of the material from the centroid, and b is the beam width.

According to Euler–Bernoulli beam theory, the angle of rotation of a beam cross section, normal to the centroid axis, is everywhere related to the slope of the deformed centroid axis as follows:

$$\theta(x, t) = \frac{\partial w(x, t)}{\partial x}, \qquad 0 \le x \le l. \tag{2}$$

For small deformations, the axial strain everywhere in the beam is

$$S_1(x, z, t) = \frac{\partial u_0(x, t)}{\partial x} - \frac{\partial^2 w(x, t)}{\partial x^2} z. \tag{3}$$

Constitutive equations. The constitutive equation for the nonactive shim material, bounded by $-h_s/2 \le z \le h_s/2$, may be written as

$$T_{1,s} = c_{11,s} S_1, \tag{4}$$

where $T_{1,s}$ is the axial stress in the shim material and $c_{11,s}$ is the modulus of elasticity of the shim material.

For the two piezoelectric layers, bounded by $h_s/2 \le z \le h/2$ and $-h/2 \le z \le -h_s/2$, the constitutive equations may be written as [Roundy et al. 2004]

$$T_{1,p} = c_{11,p} S_1 - e_{31,p} E_{3,p}, \qquad D_{3,p} = e_{31,p} S_1 + \varepsilon_{33,p} E_{3,p}, \tag{5}$$

where $T_{1,p}$ is the axial stress in the piezoelectric material, $c_{11,p}$ is the elastic constant of the piezoelectric material, $\varepsilon_{33,p}$ is the permittivity in the thickness direction, $d_{31,p}$ is the piezoelectric constant, $E_{3,p}$ is the electric field in the thickness direction, and $D_{3,p}$ is the electric displacement in the thickness direction.

A bimorph piezoelectric beam in the {3-1} mode is made of two identical piezoelectric layers at the top and bottom and a shim in the middle, which makes the structure a symmetrically laminated beam. In a symmetrically laminated beam, the axial stretching does not induce bending, and vice versa. For a composite beam of very large length-to-thickness ratios, the dominating strains and stresses in each constitutive layer are the axial strains and stresses due to the bending and axial stretching when it is operated in the vicinity of the fundamental natural frequency of the in-plane bending. Other stress components, for example the transverse shear stress, are negligible.

For piezoelectric composite beams of moderate or large thickness, the electrical field in a piezoelectric layer may vary considerably in the thickness direction [Wang et al. 2007]. However, for a very thin piezoelectric laminate, the electrical field across each piezoelectric layer may be considered constant in the thickness direction. In this paper, the piezoelectric structure is thin and symmetric. The following simplified relationship between the electric field and the voltage differential (v) across a single piezoelectric

layer is employed:

$$E_{3,p} = \begin{cases} -v/h_p & \text{if } h_s \le 2z \le h, \\ 0 & \text{if } -h_s \le 2z \le h_s, \\ v/h_p & \text{if } -h \le 2z \le -h_s, \end{cases} \tag{6}$$

where h_p is the thickness of the top or bottom piezoelectric layer and v is the voltage across one piezoelectric layer.

Motion analysis. A rigid proof mass is commonly attached to the beam at the free end to enhance power generation. When the beam-mass system is clamped to a rigid moving base, the beam-mass system participates in two motions: the rigid body motion with the base and the elastic motion relative to the base. The rigid reference motion is responsible for providing an excitation in the form of a distributed inertial force field. The relative elastic motion is desired to yield necessary straining of materials for producing electrical charges.

A beam-mass system is capable of various types of elastic deformations when the excitation frequencies vary considerably. They include bending, axial stretching/compression, and torsion. However, when the system is excited in the vicinity of the fundamental natural frequency, the beam motion is predominantly bending in the x-z coordinate plane. The proof mass motion is of the type of general plane motion. Since the lateral motion is coupled to the lateral bending motion for nonsymmetric attachments of the proof mass, the longitudinal deformation and lateral bending are considered. Bending in the y-z coordinate plane and torsion about the z axis are negligible.

To determine the deformations of a flexible beam at time t, a set of moving coordinates fixed to the moving ground are employed. For translational base motion in the vertical direction, the base-fixed coordinate translates with velocity $\dot{v}_b$. A material point P, located a distance x from the reference point on the neutral axis before deformations, as shown in Figure 2, moves to P' after deformations. If the

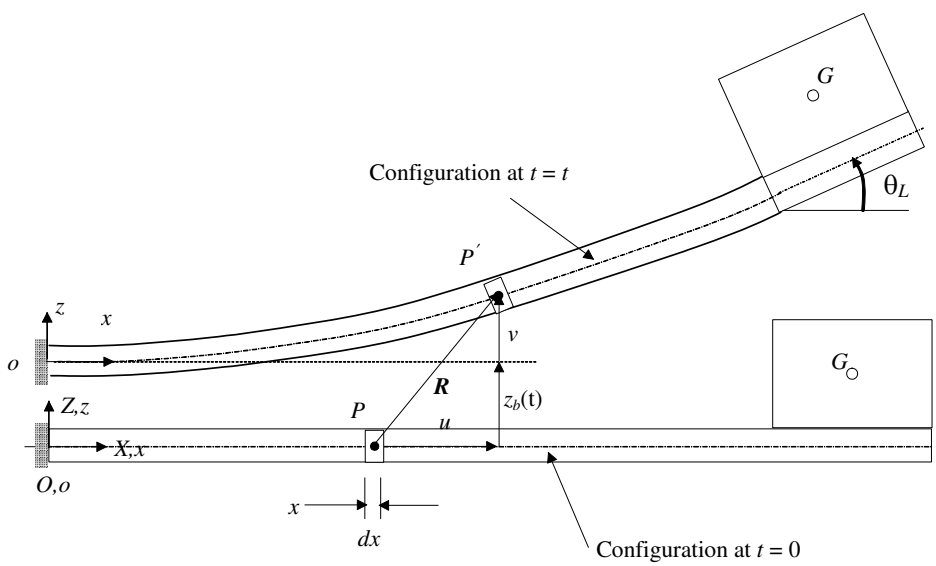

Figure 2. Sketch of deformed piezoelectric structure with respect to the reference configuration.

longitudinal and lateral displacements measured with respect to the body-fixed coordinate system x-z are $u(x,t)$ and $w(x,t)$, respectively, the absolute position of P' may be written in terms of the base-fixed coordinates as

$$\boldsymbol{R} = \{\boldsymbol{e}_x \;\; \boldsymbol{e}_y\} \begin{Bmatrix} x + u_0(x,t) \\ w_b(t) + w(x,t) \end{Bmatrix}, \tag{7}$$

where $\boldsymbol{R}_o$ is the rigid-body position vector of reference point o, and $\boldsymbol{e}_x$ and $\boldsymbol{e}_y$ are the two unit vectors of the base-fixed coordinate system. For a nonrotating base motion, these two unit vectors are constant and identical to the unit vectors in the space-fixed coordinates.

The velocity of point P' may be written in the body-fixed coordinate system as

$$\dot{\boldsymbol{R}} = \{\boldsymbol{e}_x \;\; \boldsymbol{e}_z\} \begin{Bmatrix} \dot{u}_0 \\ \dot{w}_b + \dot{w} \end{Bmatrix}, \tag{8}$$

where $\dot{w}_b$ is the velocity of the vibrating base and $\dot{u}_0$ and $\dot{w}$ are the time rates of longitudinal and lateral deflections with respect to the moving coordinate system.

Kinetic energy. The kinetic energy of the dynamical system may be conveniently written as

$$T = T_{\text{beam}} + T_{\text{mass}}, \tag{9}$$

where T_{beam} is the kinetic energy of the beam and T_{mass} is the kinetic energy of the proof mass plus the portion of the beam bonded to the mass.

The kinetic energy of the beam may be written as

$$T_{\text{beam}} = \underbrace{\frac{1}{2}\int_0^l \bar{m}\dot{R}^2\,dx}_{\text{translational}} + \underbrace{\frac{1}{2}\int_0^l \bar{i}_y\dot{\theta}^2\,dx}_{\text{rotational}}, \tag{10}$$

where $\bar{m}$ is the mass of the beam per unit length, $\bar{i}_y$ is the mass moment of inertia of the beam about the y-axis per unit length, and $\dot{\theta}$ is the rate of the angle of rotation of a plane normal to the centroid. For a symmetrically laminated beam of constant width b, we can compute $\bar{m}$ and $\bar{i}_y$ by

$$\bar{m} = \sum_{k=1}^{n} \rho_k h_k b, \qquad \bar{i}_y = \frac{1}{3}\sum_{k=1}^{n} \rho_k b\{(z_2^{(k)})^3 - (z_1^{(k)})^3\}, \tag{11}$$

where $z_1^{(k)}$ and $z_2^{(k)}$ are the z-coordinates of the lower and upper faces of k-th layer, ρ_k is the density of the material in k-th layer, and h_k is the thickness of k-th layer. For large length-to-thickness ratios, the rotary inertia of the beam bimorph is very small, and will be ignored in this paper.

The kinetic energy of the proof mass attached to the free end of the piezoelectric beam structure may be written as

$$T_{\text{mass}} = \tfrac{1}{2}m[\dot{X}_G^2 + \dot{Z}_G^2] + \tfrac{1}{2}J_{G,y}\dot{\theta}_l^2, \tag{12}$$

where $\dot{X}_G$ and $\dot{Z}_G$ are the velocities of the proof mass center along the x and z directions respectively, $J_{G,y}$ is the mass moment of inertia of the proof mass about the y_G axis, m is the mass of the proof mass, and $\dot{\theta}_l$ is the angle of rotation of the beam at $x = l$.

At a given instant, the proof mass center is related to the beam deflection as

$$X_G = u_{0,l} + a_G\cos\theta_l - c_G\sin\theta_l, \qquad Y_G = w_b + w_l + a_G\sin\theta_l + c_G\cos\theta_l, \tag{13}$$

where a_G and c_G are the axial and lateral distances, respectively, of proof mass center (G) with reference to the end point of the beam neutral axis at $x = l$, and $u_{0,l}$ and w_l are the axial and lateral deformations of the beam at $x = l$.

Finally, the kinetic energy of the proof mass may be written as

$$T_{\text{mass}} = \tfrac{1}{2} m(\dot{X}_G^2 + \dot{Y}_G^2) + \tfrac{1}{2} J_{G,y} \dot{\theta}_l^2. \tag{14}$$

Strain energy. The strain energy of the composite beam associated with the longitudinal and lateral deformations is

$$\begin{aligned} V &= \frac{1}{2}\int_{V_p} T_{1,p} S_1 \, dV_p + \frac{1}{2}\int_{V_s} T_{1,s} S_1 \, dV_s \\ &= \frac{1}{2}\int_{V_p} c_{11,p} (S_1)^2 \, dV_p + \frac{1}{2}\int_{V_p} e_{31} h_p^{-1} \upsilon S_1 \, dV_p + \frac{1}{2}\int_{V_s} c_{11,s} (S_1)^2 \, dV_s, \end{aligned} \tag{15}$$

where V_s is the volume of the shim material and V_p is the volume of the piezoelectric material.

Substituting (3) into (15), the strain energy for the symmetrically laminated composite beam may be expressed in terms of a line integral as

$$V = \frac{1}{2}\int_0^l R_u \left(\frac{\partial u_0}{\partial x}\right)^2 dx + \frac{1}{2}\int_0^l R_w \left(\frac{\partial^2 w}{\partial x^2}\right)^2 dx - \frac{1}{2}\int_0^l \gamma \frac{\partial^2 w}{\partial x^2} \upsilon \, dx, \tag{16}$$

where

$$\begin{aligned} &R_u = 2c_{11,p} 2A_p + c_{11,s} A_s, && R_w = c_{11,p} I_p + c_{11,s} I_s, && \gamma = 2e_{31} A_p \bar{z}_p h_p^{-1}, && A_p = \tfrac{1}{2} b(h - h_s), \\ &A_s = bh_s, && I_p = \tfrac{1}{12} b(h^3 - h_s^3), && I_s = \tfrac{1}{12} b h_s^3, && \bar{z}_p = \tfrac{1}{4}(h + h_s). \end{aligned}$$

Electrical energy. The electrical energy in the two layers of piezoelectric material may be written as

$$W_e = \frac{1}{2}\int_{V_p} E_3 D_3 dV = \frac{1}{2}\int_0^l \gamma \upsilon \frac{\partial^2 w}{\partial x^2} dx + 2\left(\frac{1}{2} c_0 \upsilon^2\right), \tag{17}$$

where $c_0 = \varepsilon_{33} b l h_p^{-1}$.

Energy dissipation. Energy loss in a vibrating piezoelectric structure can be handled mathematically if it is in a form of proportionality damping. The proportionality damping accounts for both the environmental damping due to the viscosity of the surrounding medium and the internal structural damping. Within the context of Lagrange equations, the Rayleigh dissipation function is an effective way of bringing damping into consideration. The energy loss function may be assumed as

$$U = \frac{1}{2}\int_0^l \alpha_u \bar{m} \dot{u}_0^2 dx + \frac{1}{2}\int_0^l \alpha_w \bar{m} \dot{w}^2 dx + \frac{1}{2}\int_0^l \beta_u R_u \left(\frac{\partial \dot{u}_0}{\partial x}\right)^2 dx + \frac{1}{2}\int_0^l \beta_w R_w \left(\frac{\partial^2 \dot{w}}{\partial x^2}\right)^2 dx, \tag{18}$$

where α_u, α_w, β_u, and β_w are proportionality constants. Their values are not determined individually. Instead, a combined damping ratio associated with a particular mode is measured and used in simulations for a specific setup.

Work done on resistor. The rate of electrical work done by the resistor per unit voltage is

$$\dot{Q}_R = \begin{cases} -i & \text{for piezoelectric layers in parallel,} \\ -2i & \text{for piezoelectric layers in series,} \end{cases} \tag{19}$$

where i is the current passing through the resistor.

The work done by the resistor per unit voltage is then

$$Q_R = \begin{cases} -q & \text{for piezoelectric layers in parallel,} \\ -2q & \text{for piezoelectric layers in series,} \end{cases} \tag{20}$$

where q is the charge flowing through the resistor.

3. Governing equations of the electromechanical system

In this section, a finite element procedure for obtaining a set of ordinary differential equations for the piezoelectric power harvesting system is presented.

Beam finite elements. The three-node beam element used in this paper has three axial nodal displacements, u_1^e, u_2^e, and u_3^e, three lateral displacements, w_1^e, w_2^e, and w_3^e, and three angles of rotation, θ_1^e, θ_2^e, and θ_3^e. To facilitate the formation of element matrices, a local axial coordinate originating at the first node of a beam element is used. For a straight beam, the local axial coordinate is related to the body-fixed coordinates by $\xi = x - x_1^e$ and $0 \le \xi \le l_e$, where x_1^e is the axial coordinate of the first node of element e and ξ is the local coordinate for element e. The longitudinal and lateral displacements of a material point within a beam finite element may be determined by the shape function and nodal variables from the equations

$$u_e = [N_1(\xi)][D_1^e]\{q_u^e\}, \quad w_e = [N_2(\xi)][D_2^e]\{q_w^e\}. \tag{21}$$

(see [Yu and Cleghorn 2002]). For convenience in assembly of component equations, the global nodal displacement vector is rearranged in the following manner:

$$\{r\} = \begin{Bmatrix} u_1 & w_1 & \theta_1 & u_2 & w_2 & \theta_2 & \dots & u_{NN} & w_{NN} & \theta_{NN} \end{Bmatrix}^T. \tag{22}$$

The longitudinal and lateral nodal displacements are related to the global displacement vector through transformation matrices $[T_u^e]$ and $[T_w^e]$ as follows:

$$\{q_u^e\} = [T_u^e]\{r\}, \quad \{q_w^e\} = [T_w^e]\{r\}. \tag{23}$$

Expressions for kinetic, strain, and dissipation and electric energies in nodal displacements. If N_e beam finite elements are used for the piezoelectric structure, the kinetic energy (excluding the rotary inertia), the strain energy, the Rayleigh dissipation energy function, and the electrical energy for the dynamical system may be written in terms of the nodal displacements and the voltage across a single layer of piezoelectric material may be written as

$$\begin{aligned} T &= \tfrac{1}{2}\{\dot{r}\}^T[M]\{\dot{r}\} + \dot{w}_b\{\dot{r}\}^T\{B\} + \tfrac{1}{2}\bar{m}l\dot{w}_b^2, & U &= \tfrac{1}{2}\{\dot{r}\}^T[C]\{\dot{r}\}, \\ V &= \tfrac{1}{2}\{r\}^T[K]\{r\} - \tfrac{1}{2}\gamma v\{r\}^T\{\Theta\}, & W_e &= \tfrac{1}{2}v\{r\}^T\{\Theta\} + 2\left(\tfrac{1}{2}c_0v^2\right), \end{aligned} \tag{24}$$

where

$$[C]=\sum_{e=1}^{NE}\Big[[T_u^e]^T\big[\alpha_u[M_u^e]+\beta_u[K_u^e]\big][T_u^e]\Big]+\sum_{e=1}^{NE}[T_w^e]^T\big[\alpha_w[M_w^e]+\beta_w[K_w^e]\big][T_w^e],$$

$$[M]=\sum_{e=1}^{NE}\Big[[T_u^e]^T[M_u^e][T_u^e]+[T_w^e]^T[M_w^e][T_w^e]\Big]+[M_{\text{mass}}],\quad [K]=\sum_{e=1}^{NE}\Big[[T_u^e]^T[K_u^e][T_u^e]+[T_w^e]^T[K_w^e][T_w^e]\Big],$$

$$\{B\}=\sum_{e=1}^{NE}[T_w^e]^T\{B_w^e\}+\{B_{\text{mass}}\},\qquad \{\Theta\}=\sum_{e=1}^{NE}[T_w^e]^T\{\Theta_w^e\},$$

$$[M_u^e]=[D_1^e]^T\left[\int_0^{l_e}\bar{m}[N_1]^T[N_1]d\xi\right][D_1^e],\quad [M_w^e]=[D_2^e]^T\left[\int_0^{l_e}\bar{m}[N_2]^T[N_2]d\xi\right][D_2^e],$$

$$[K_u^e]=[D_1^e]^T\left[\int_0^{l_e}R_u[N_1']^T[N_1']d\xi\right][D_1^e],\quad [K_w^e]=[D_2^e]^T\left[\int_0^{l_e}R_w[N_2'']^T[N_2'']d\xi\right][D_2^e],$$

$$\{\Theta\}=[D_2^e]^T\left\{\int_0^{l_e}[N_2'']^T\,d\xi\right\},\qquad \{B_w^e\}=[D_2^e]^T\left[\int_0^{l_e}\bar{m}[N_2]^T\,d\xi\right],$$

$$[M_{\text{mass}}]=\begin{bmatrix}\mathbf{0} & \mathbf{0}\\ \mathbf{0} & [\bar{M}_{\text{mass}}]\end{bmatrix},\qquad [\bar{M}_{\text{mass}}]=\begin{bmatrix}m & 0 & -mc_G\\ 0 & m & ma_G\\ -mc_G & ma_G & \bar{J}_y\end{bmatrix},$$

$$\{B_{\text{mass}}\}=\begin{Bmatrix}0 & 0 & \dots & 0 & m & ma_G\end{Bmatrix}^T,\qquad \bar{J}_y=ma_G^2+mc_G^2+J_{G,y}.$$

Governing equations. The Lagrangian for the electromechanical system may now be written as

$$L=T-V+W_e=\tfrac{1}{2}\{\dot{r}\}^T[M]\{\dot{r}\}-\tfrac{1}{2}\{q\}^T[K]\{r\}+\gamma\{r\}^T\{\Theta\}v+2\big(\tfrac{1}{2}c_0v^2\big). \tag{25}$$

Two sets of governing equations for the electromechanical system can be derived from the following Lagrange equations:

$$\frac{d}{dt}\frac{\partial L}{\partial\{\dot{r}\}^T}+\frac{\partial U}{\partial\{\dot{r}\}^T}-\frac{\partial L}{\partial\{r\}^T}=\mathbf{0},\qquad \frac{d}{dt}\frac{\partial L}{\partial\dot{v}}-\frac{\partial L}{\partial v}=Q_R. \tag{26}$$

Substituting (25) into (26), the equations of motion of the piezoelectric structure and the equation of the electrical power generation are written as

$$[M]\{\ddot{r}\}+[C]\{\dot{r}\}+[K]\{r\}-\gamma[\Theta]v=-\{B\}\ddot{w}_b,\qquad \gamma[\Theta]^T\{r\}+2c_0v=Q_R. \tag{27}$$

When the electrical output from the piezoelectric structure is connected to a resistor load and the two piezoelectric layers are connected in parallel, the voltage is related to the rate of charge as $v=R\dot{q}$. Incorporating the above electrical boundary condition and the first relation in (20) into (27), the governing equations for the coupled electromechanical system may be rewritten in terms of the mechanical displacements and the electric charge, for a sinusoidal base motion, $w_b=A\sin(\omega t+\phi)$, as follows:

$$\begin{bmatrix}[M] & \mathbf{0}\\ \mathbf{0} & 0\end{bmatrix}\begin{Bmatrix}\{\ddot{r}\}\\ \ddot{q}\end{Bmatrix}+\begin{bmatrix}[C] & -\gamma R[\Theta]\\ \mathbf{0} & R\end{bmatrix}\begin{Bmatrix}\{\dot{r}\}\\ \dot{q}\end{Bmatrix}+\begin{bmatrix}K & \mathbf{0}\\ [\Theta]^T\frac{\gamma}{2c_0} & \frac{1}{2c_0}\end{bmatrix}\begin{Bmatrix}\{r\}\\ q\end{Bmatrix}=A\omega^2\sin(\omega t+\phi)\begin{Bmatrix}\{B\}\\ 0\end{Bmatrix}. \tag{28}$$

Equation (28) is valid for two piezoelectric layers connected in parallel. The voltages across the two piezoelectric layers are each equal to the voltage across the resistor.

In the case where the two piezoelectric layers are connected in series, the voltage across the resistor is twice the voltage across each piezoelectric layer, that is, $v = R\dot{q}/2$. In the case of a series connection, one obtains the following governing equations for the electromechanical system:

$$\begin{bmatrix} [M] & \mathbf{0} \\ \mathbf{0} & 0 \end{bmatrix} \begin{Bmatrix} \{\ddot{r}\} \\ \ddot{q} \end{Bmatrix} + \begin{bmatrix} [C] & -[\Theta]\gamma\dfrac{R}{2} \\ \mathbf{0} & R \end{bmatrix} \begin{Bmatrix} \{\dot{r}\} \\ \dot{q} \end{Bmatrix} + \begin{bmatrix} K & \mathbf{0} \\ [\Theta]^T\dfrac{\gamma}{c_0} & \dfrac{2}{c_0} \end{bmatrix} \begin{Bmatrix} \{r\} \\ q \end{Bmatrix} = A\omega^2 \sin(\omega t + \phi) \begin{Bmatrix} \{B\} \\ 0 \end{Bmatrix}. \quad (29)$$

Handling mechanical boundary conditions. If the base is considered rigid, the piezoelectric beam is clamped to the base. The axial displacement, the lateral displacement, and the angle of rotation of the beam with respect to the base are zero. The boundary conditions at the clamping end can be easily handled using the elimination method or the penalty method [Bathe 1995]. In this paper, the elimination method is employed. It is noted that other boundary conditions, such as elastically restrained edges simulating less than rigid constraints between the base and the beam, can also be handled in the frame work of the finite element formulation.

Deleting the first three equations and the first three nodal variables in the remaining equations in (28), the governing equations for the electromechanical system, which satisfy all electrical and mechanical boundary conditions for the parallel connection of the two piezoelectric layers, may now be written as

$$\begin{bmatrix} [\tilde{M}] & \mathbf{0} \\ \mathbf{0} & 0 \end{bmatrix} \begin{Bmatrix} \{\ddot{\tilde{r}}\} \\ \ddot{q} \end{Bmatrix} + \begin{bmatrix} [\tilde{C}] & -\gamma R[\tilde{\Theta}] \\ \mathbf{0} & R \end{bmatrix} \begin{Bmatrix} \{\dot{\tilde{r}}\} \\ \dot{q} \end{Bmatrix} + \begin{bmatrix} \tilde{K} & \mathbf{0} \\ [\tilde{\Theta}]^T\dfrac{\gamma}{2c_0} & \dfrac{1}{2c_0} \end{bmatrix} \begin{Bmatrix} \{\tilde{r}\} \\ q \end{Bmatrix} = A\omega^2 \sin(\omega t + \phi) \begin{Bmatrix} \{\tilde{B}\} \\ 0 \end{Bmatrix}, \quad (30)$$

where matrices with a tilde on top are the result of their corresponding matrices with the first three rows and columns deleted, and vectors with a tilde are the result of their corresponding vectors with the first three elements deleted.

Similarly, Equation (29) for the series connection of the two piezoelectric layers can also be modified to satisfy the boundary condition at the clamped end. The governing equations for the coupled electromechanical system may be written as

$$\begin{bmatrix} [\tilde{M}] & \mathbf{0} \\ \mathbf{0} & 0 \end{bmatrix} \begin{Bmatrix} \{\ddot{\tilde{r}}\} \\ \ddot{q} \end{Bmatrix} + \begin{bmatrix} [\tilde{C}] & -[\tilde{\Theta}]\dfrac{\gamma R}{2} \\ \mathbf{0} & R \end{bmatrix} \begin{Bmatrix} \{\dot{\tilde{r}}\} \\ \dot{q} \end{Bmatrix} + \begin{bmatrix} \tilde{K} & \mathbf{0} \\ [\tilde{\Theta}]^T\dfrac{\gamma}{c_0} & \dfrac{2}{c_0} \end{bmatrix} \begin{Bmatrix} \{\tilde{r}\} \\ q \end{Bmatrix} = A\omega^2 \sin(\omega t + \phi) \begin{Bmatrix} \{\tilde{B}\} \\ 0 \end{Bmatrix}. \quad (31)$$

Equation (30) for the coupled electromechanical system can be written in a unified manner as

$$[M_{\text{em}}]\{\ddot{x}_{\text{em}}\} + [C_{\text{em}}]\{\dot{x}_{\text{em}}\} + [K_{\text{em}}]\{x_{\text{em}}\} = \{F_{\text{em}}\}\sin(\omega t + \phi), \quad (32)$$

where the subscript em in the above equations stands for electromechanical. Other quantities are defined as follows for the two piezoelectric layers in parallel:

$$[M_{\text{em}}] = \begin{bmatrix} [\tilde{M}] & \mathbf{0} \\ \mathbf{0} & 0 \end{bmatrix}, [C_{\text{em}}] = \begin{bmatrix} [\tilde{C}] & -\gamma R[\tilde{\Theta}] \\ \mathbf{0} & R \end{bmatrix}, [K_{\text{em}}] = \begin{bmatrix} \tilde{K} & \mathbf{0} \\ [\tilde{\Theta}]^T\dfrac{\gamma}{2c_0} & \dfrac{1}{2c_0} \end{bmatrix}, \{x_{\text{em}}\} = \begin{Bmatrix} \{\tilde{r}\} \\ q \end{Bmatrix}, \{F_{\text{em}}\} = A\omega^2 \begin{Bmatrix} \{\tilde{B}\} \\ 0 \end{Bmatrix}.$$

For the two piezoelectric layers in series, the electromechanical mass matrix and the load vector are identical to those given above. However, the electromechanical damping matrix and the electromechanical stiffness matrix are different and are given as:

$$[C_{\mathrm{em}}] = \begin{bmatrix} [\tilde{C}] & -[\tilde{\Theta}]\dfrac{\gamma R}{2} \\ \mathbf{0} & R \end{bmatrix}, \qquad [K_{\mathrm{em}}] = \begin{bmatrix} \tilde{K} & \mathbf{0} \\ [\tilde{\Theta}]^T \dfrac{\gamma}{c_0} & \dfrac{2}{c_0} \end{bmatrix}.$$

Steady-state solution. A steady-state solution to (32) may be sought in the following manner:

$$\{x_{\mathrm{em}}\} = \{X\}_c \cos(\omega t + \phi) + \{X\}_s \sin(\omega t + \phi), \tag{33}$$

where $\{X\}_c$ and $\{X\}_s$ are constant vectors.

Substituting (33) into the governing differential equations and comparing the coefficients associated with the cosine and sine harmonics, one obtains the following set of inhomogeneous algebraic equations for the two unknown vectors:

$$\begin{bmatrix} [K_{\mathrm{em}}] - [M_{\mathrm{em}}]\omega^2 & [C_{\mathrm{em}}]\omega \\ -[C_{\mathrm{em}}]\omega & [K_{\mathrm{em}}] - [M_{\mathrm{em}}]\omega^2 \end{bmatrix} \begin{Bmatrix} \{X\}_c \\ \{X\}_s \end{Bmatrix} = \begin{Bmatrix} \mathbf{0} \\ \{F_{\mathrm{em}}\} \end{Bmatrix}. \tag{34}$$

Once $\{X\}_c$ and $\{X\}_s$ are determined, the amplitudes for the mechanical variables (nodal displacements) and the electrical variable can be computed. A postprocessing scheme can be employed to obtain the amplitudes for the current, voltage and power. It is noted that there are two ways to determine the power output: the peak power and the average power. For the sinusoidally varying current and voltage across an electrical load, the average power is one half of the peak power.

For a piezoelectric system under sinusoidal base motion, (34) can be used to obtain the mechanical and electrical responses provided that the damping ratio accounts for the loss of energy in the form of structural damping. For small scale vibration, the air resistance is negligible.

4. Validation of the proposed model

The model proposed in this paper is validated by comparing the simulation results obtained using the model with the experimental results of two piezoelectric bimorph beam power harvesters. One design, with the two piezoelectric layers connected in series and a proof mass simplified as a point mass, is available in the literature. The other design, with the two piezoelectric layers connected in parallel and a proof mass which cannot be simplified as a point mass, is built and tested in this paper for investigating the effect of the mass moment of inertia and mass center offset.

A cantilever piezoceramic structure carrying a point mass. The first system, sketched in Figure 3, is a piezoceramic harvester developed in [Erturk and Inman 2009]. The dimensions of the proof mass in the

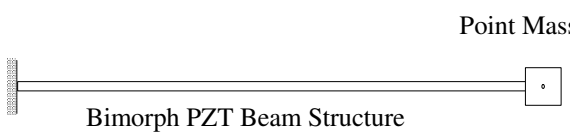

Figure 3. Sketch of the piezoelectric structure carrying a small point mass.

plane of base motion are relatively small and thus it is treated as a point mass. The two piezoelectric layers are connected in a series manner to power a resistive load.

To validate the finite element model described in this paper, simulations were conducted for four different meshing schemes. The bimorph piezoelectric beam consists of a shim core of brass and two layers of piezoceramic materials. Parameters for the piezoelectric power harvester are given in Table 1 for reference. The proof mass is treated as a point mass, that is, the effects of the mass moment of inertia and the mass center offset are ignored in this paper and in [Erturk and Inman 2009]. An electrical load of $R = 470\,\mathrm{k}\Omega$ was used. The peak powers, peak voltages, and optimal frequencies, obtained using one, two, four, and seven beam finite elements, are given in Table 2. Here the optimal frequencies are the frequencies at which a maximum power (or voltage) is generated for a given resistive load and base excitation amplitude. It can be seen that the results converge rapidly if four or more elements are

Parameters	Symbol	Values
Piezoelectric structure		
Length (mm)	l	50.8
Width (mm)	b	31.8
Damping ratio	ζ	0.027
Shim material (brass)		
Thickness (mm)	t_s	0.14
Modulus of elasticity (GPa)	E_s	105
Shim density (kg/m^3)	ρ_s	9000
Piezoelectric material (PZT-5A)		
Thickness of each piezoelectric layer (mm)	t_p	0.26
Modulus of elasticity (GPa)	E_p	66
Density (kg/m^3)	ρ_p	7800
Piezoelectric constant (pm/V)	d_{31}	190
Piezolayer permittivity (F/m)	ε_{33}	$1500\varepsilon_0$
Proof mass		
Mass (g)	m	12.0
Mass moment of inertia (kg m^2)	J_G	0
Mass center x-location (mm)	a_G	0
Mass center z-location (mm)	c_G	0
Base motion (harmonic)		
Acceleration magnitude (m/s^2)	A	1 g or 9.81
Frequency range for testing (Hz)	ω or f	30–70

Table 1. Parameters for a bimorph piezoelectric harvester carrying a small proof mass [Erturk and Inman 2009]. The finite element model has $N_e = 7$ elements, except for convergence studies, where different numbers of finite elements were used. The resistance $\boldsymbol{R}$ of the resistor is variable. The two piezoelectric layers are connected in series.

Number of beam elements used	Peak power (mW)	Peak voltage (V)	Optimal frequency (Hz)
1	18.470	93.170	48.040
2	18.479	93.194	48.050
4	18.470	93.170	48.050
7	18.470	93.170	48.050

Table 2. Convergence studies for a bimorph beam of [Roundy et al. 2004] for $R = 470\,\text{k}\Omega$.

used. Based on this, seven beam finite elements are used for all simulations in this paper. Use of an unnecessarily large number of elements is not desired for bimorph beams of small length-to-width ratios (about 1.6 for the bimorph beam used in [Erturk and Inman 2009]).

For $R = 470\,\text{k}\Omega$, the experimental peak powers of [Erturk and Inman 2009] were digitized and plotted against the simulation results obtained using the procedure proposed in this paper. It can be seen from Figure 4 that the simulation results are in good agreement with the data of [Erturk and Inman 2009].

A cantilever piezoelectric power harvester with a nonpoint mass. The second power harvester, designed, fabricated, and tested in this paper, is shown in Figure 5. In this design, the mass moment of inertia and mass center offset of the proof mass contribute significantly to the structural natural frequencies and the electrical power generation. Thus the mass cannot be treated as a point mass. The power harvester is tested on a vibration shaker. The shaker is made to vibrate sinusoidally with a peak acceleration amplitude of 0.5 g and adjustable excitation frequencies (20–120 Hz). The entire experimental setup,

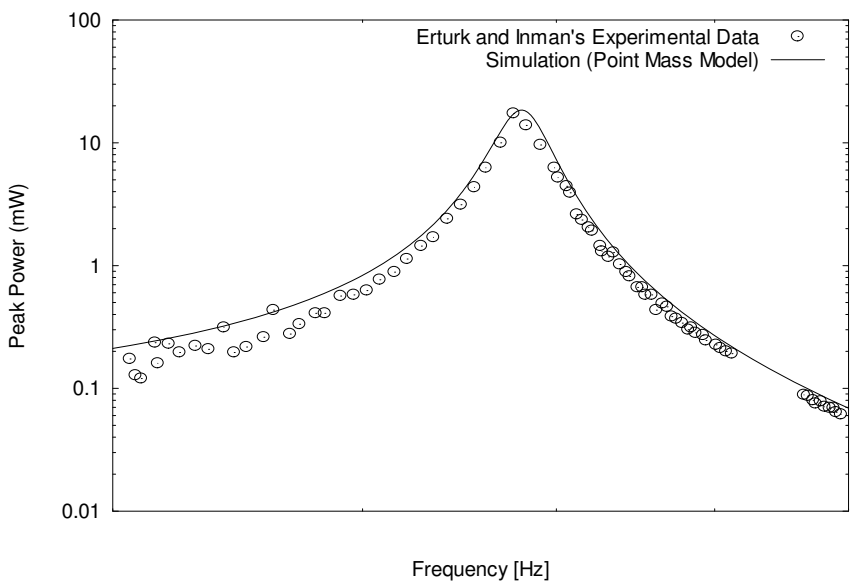

Figure 4. Comparison of simulated peak power outputs with the experimental data in [Erturk and Inman 2009] for $R = 470\,\text{k}\Omega$.

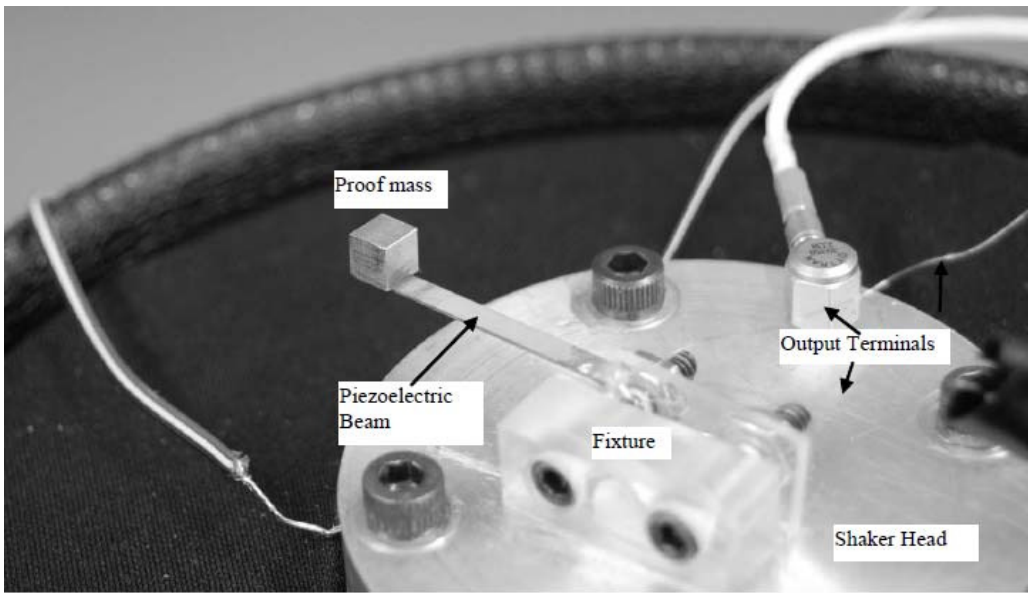

Figure 5. Photograph of the piezoelectric structure carrying a large proof mass.

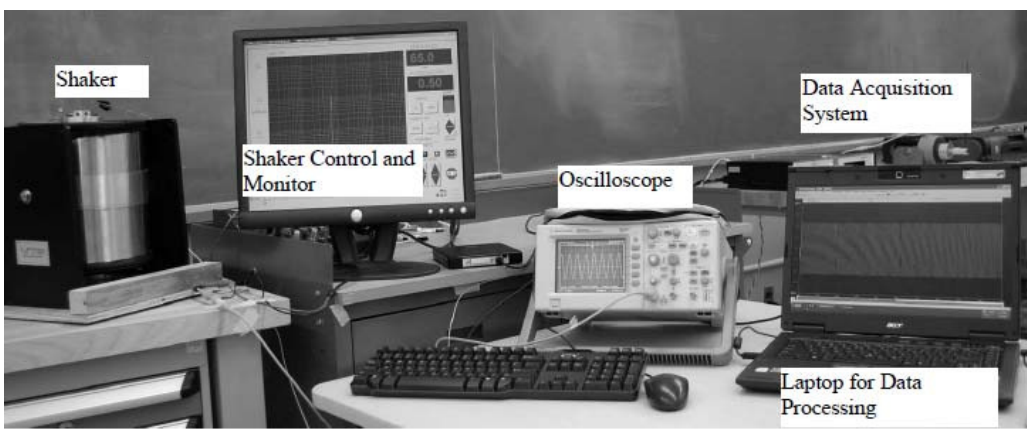

Figure 6. Photograph of the entire experimental setup.

consisting of the shaker, the piezoelectric harvester, a resistor load, a digital oscilloscope, and a data acquisition system, is shown in Figure 6.

The average power outputs for frequencies between 20 Hz and 120 Hz were measured and computed using the procedure described in the previous section for six different electric loads (20, 70, 150, 250, 350, and 500 kΩ). Two proof mass models, the comprehensive mass model and the point mass model, were used in the simulations. The comprehensive model takes into consideration the mass, mass moment of inertia, axial offset, and vertical offset of the mass center with respect to the bimorph beam and mass interface. The point mass model takes into consideration only the mass concentrated at the beam-mass interface. In an impact test, the damping ratio was found to be 0.024 for the experimental setup.

This damping ratio is used for all simulations. According to Figure 7, for all six resistive loads, the comprehensive model yields a good match with the experimental data while the point mass model leads to significant discrepancy between the calculated results and the experimental data in terms of resonant frequencies and the generated power.

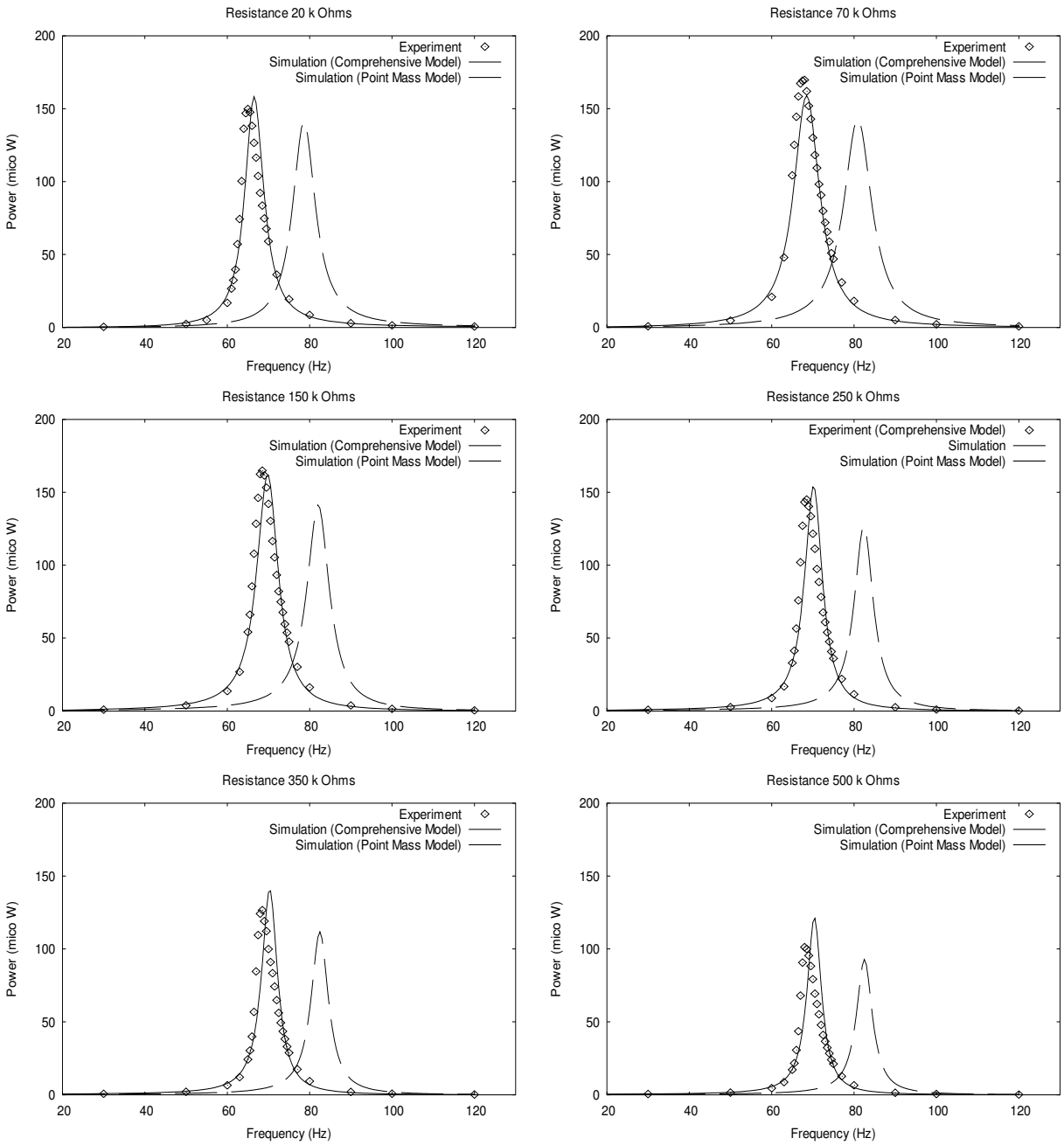

Figure 7. Comparisons of simulated average power outputs with experimental data for ranges of excitation frequencies and electrical loads.

5. Effects of the dimension and geometry of the proof mass on power output

To reduce the overall dimensions, heavy materials such as tungsten are commonly used to make the proof mass for a cantilever-based bimorph piezoelectric structure. However, this reduction does not validate the use of a point model. In this section, the effects on power generation when different proof masses are attached are investigated for the piezoelectric system described in Table 3. The system is excited by sinusoidal base motion with a 0.5 g acceleration magnitude and variable frequencies.

Four different configurations of proof masses of parallelepiped shapes, as shown in Figure 8, are studied. These mass shapes and attachments are used in typical designs in the literature. All masses have a dimension of 5 mm in the y-direction. The first three masses have their mass centers located at the beam neutral axis. There is only a horizontal offset between the proof mass center and the structure-mass

Parameters	Symbol	Values
Piezoelectric structure		
Length (mm)	l	21.85
Width (mm)		3.2
Damping ratio (1st mode)	ζ	0.024
Shim material (brass)		
Thickness (mm)	t_s	0.102
Modulus of elasticity (GPa)	E_s	100
Shim density (kg/m^3)	ρ_s	8.4
Piezoelectric material (PZT-5E)		
Thickness of each piezoelectric layer (mm)	t_p	0.139
Modulus of elasticity (GPa)	E_p	62
Density (kg/m^3)	ρ_p	7800
Piezoelectric constant (m/V)	d_{31}	0.320×10^{-9}
Piezolayer permittivity (F/m)	ε_{33}	3.364×10^{-8}
Proof mass		
Mass (kg)	m	0.975×10^{-3}
Mass moment of inertia (kg m^2)	J_G	0.406×10^{-8}
Length (mm)	a	5
Width (mm)	b	5
Height (mm)	c	5
Base motion (harmonic)		
Acceleration magnitude (m/s^2)	A	4.905
Frequency range for testing (Hz)	ω or f	20–120

Table 3. Parameters for an experimental bimorph piezoelectric harvester carrying a large proof mass on top. The resistance $\boldsymbol{R}$ of the resistor is variable. The finite element model has $N_e = 7$ elements. The two piezoelectric layers are connected in parallel.

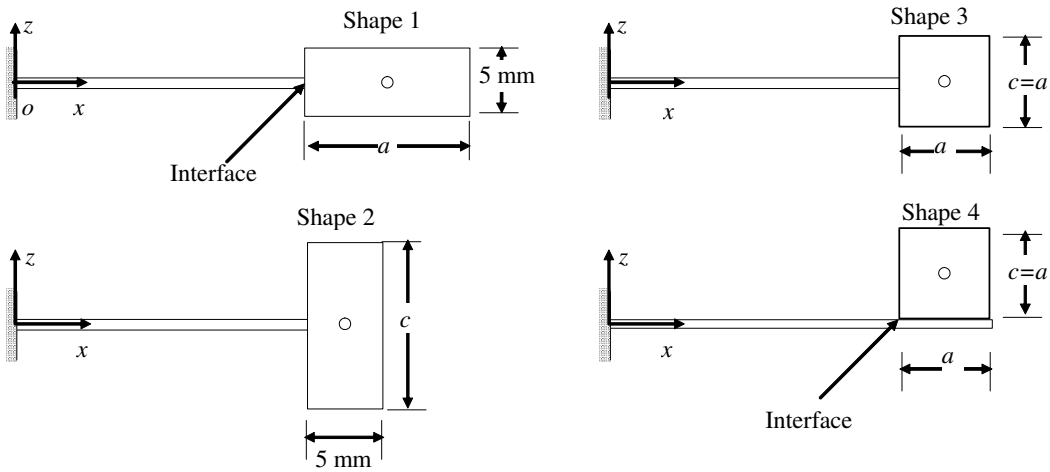

Figure 8. Four different proof masses and configurations. All parallelepiped proof masses have a thickness of 5 mm in the y-direction.

interface. The fourth mass is placed on top of the beam, and therefore has both a horizontal and a vertical offset between the proof mass center and the structure-mass interface. From the mass matrix composition in the governing equations, the vertical offset, c_G, couples the axial deformation and vertical bending. The presence of a nonzero vertical offset requires that the axial deformation be considered. Overall, the point mass model, in which the mass moment of inertia and the mass center offset are ignored, tends to overpredict the structural natural frequencies. As a result, when the piezoelectric structure is connected to a resistive load, the resonant frequency of the electromechanical system is shifted upwards.

The results shown in Figure 9 indicate that the fundamental natural frequencies vary considerably with the characteristic dimension of the four masses. The point mass model yields acceptable results only when the overall dimensions of the proof mass in the x-z plane are small. This is especially true for the third and fourth shapes, which have a square aspect ratio; the proof masses shrink to a point if the characteristic dimensions (lengths and heights) reduce to zero. However, for the first shape, the characteristic dimension of the proof mass is the length with a fixed height of 5 mm; the natural frequencies do not quite converge to those for a point mass. For the second proof mass shape, the point mass model does not yield satisfactory results even if the characteristic dimension (height) approaches zero.

Accurate predictions of power generation from a beam-mass cantilever piezoelectric system depend strongly on the reliable prediction of the structural natural frequencies. Errors in predicting the structural natural frequencies will result in errors in power generation. The simulated power outputs in the frequency range 0–200 Hz are shown in Figure 10 for parallel connection and a resistive load of $R = 70\,\text{k}\Omega$ for the piezoelectric structure defined in Table 3. It can be seen clearly from the simulation results that the proof mass dimension and geometry shift the occurrence of peak powers considerably. It is noted that for the fourth shape, the second spike corresponding to the second resonant frequency appears at 180 Hz from the comprehensive model.

According to the above simulations and analysis, the mass moment of inertia, axial offset, and vertical offset of the mass center due to the nonnegligible dimension and the geometry of the proof mass have

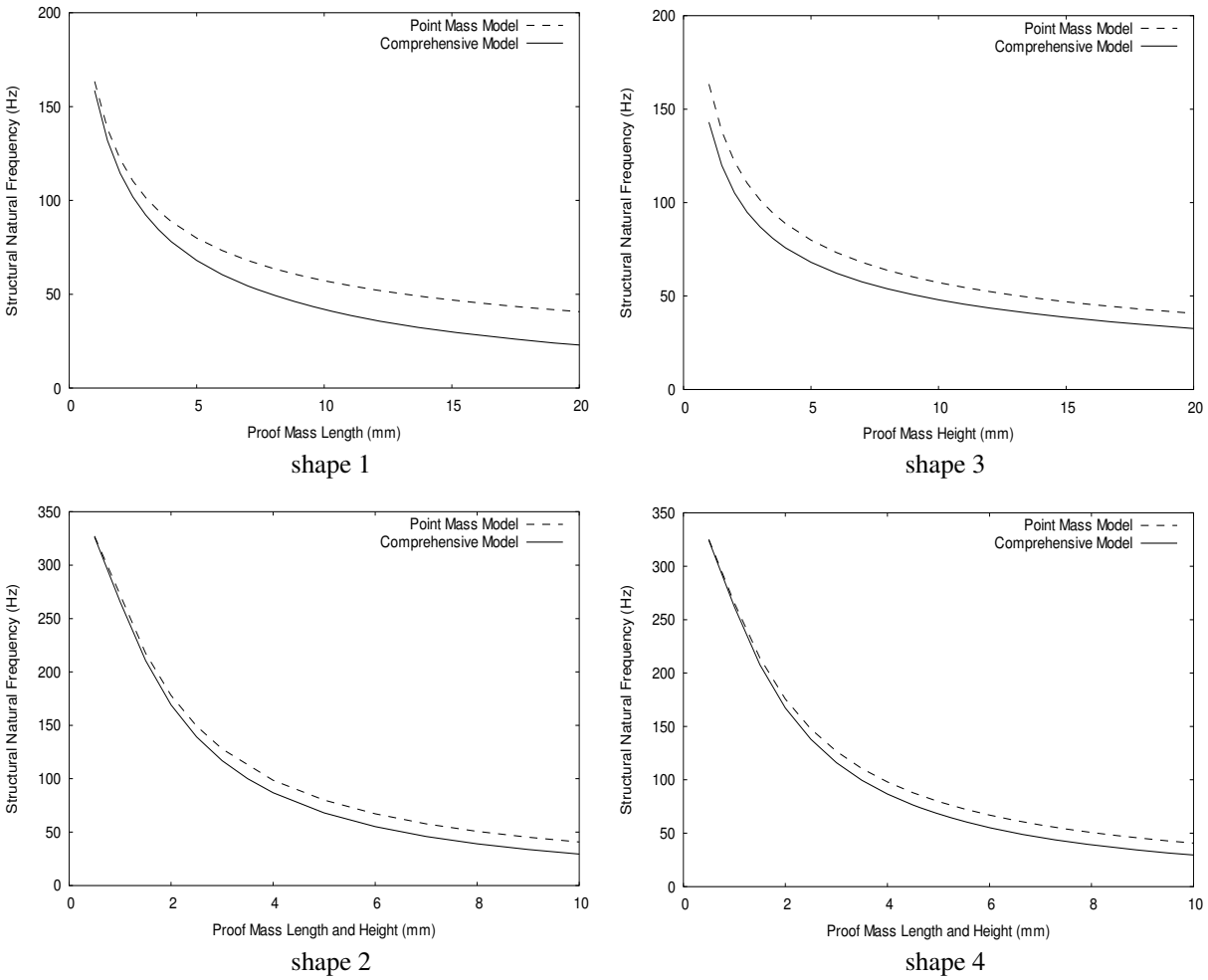

Figure 9. Effects of proof masses and configurations on structural natural frequencies.

significant effects on the resonant frequency of the piezoelectric beam power harvesters and the output power. The comprehensive finite element model presented in this paper can readily take the effects of the proof mass dimension and geometry into consideration and thus is able to accurately predict the performance of piezoelectric power harvesters. However, it can be very difficult to consider those effects in analytical models or equivalent circuit models. As a result, the comprehensive finite element model is more advantageous than the simplified analytical model in simulating piezoelectric power harvesters.

For the block type proof mass photographed in Figure 5, the resonant frequencies predicted by the comprehensive model are in excellent agreement with the experimental resonant frequencies for a wide range of resistive loads. However, the point mass model overpredicts the resonant frequencies by 18%. As for the peak powers and voltages, the errors of predicted values using the point mass model vary with the resistive loads. At 70 kΩ, the point mass model underpredicts the peak power by 9.5%. It should be pointed out here that, for proof masses of complex configurations, the predictions of the point mass model may be completely unacceptable.

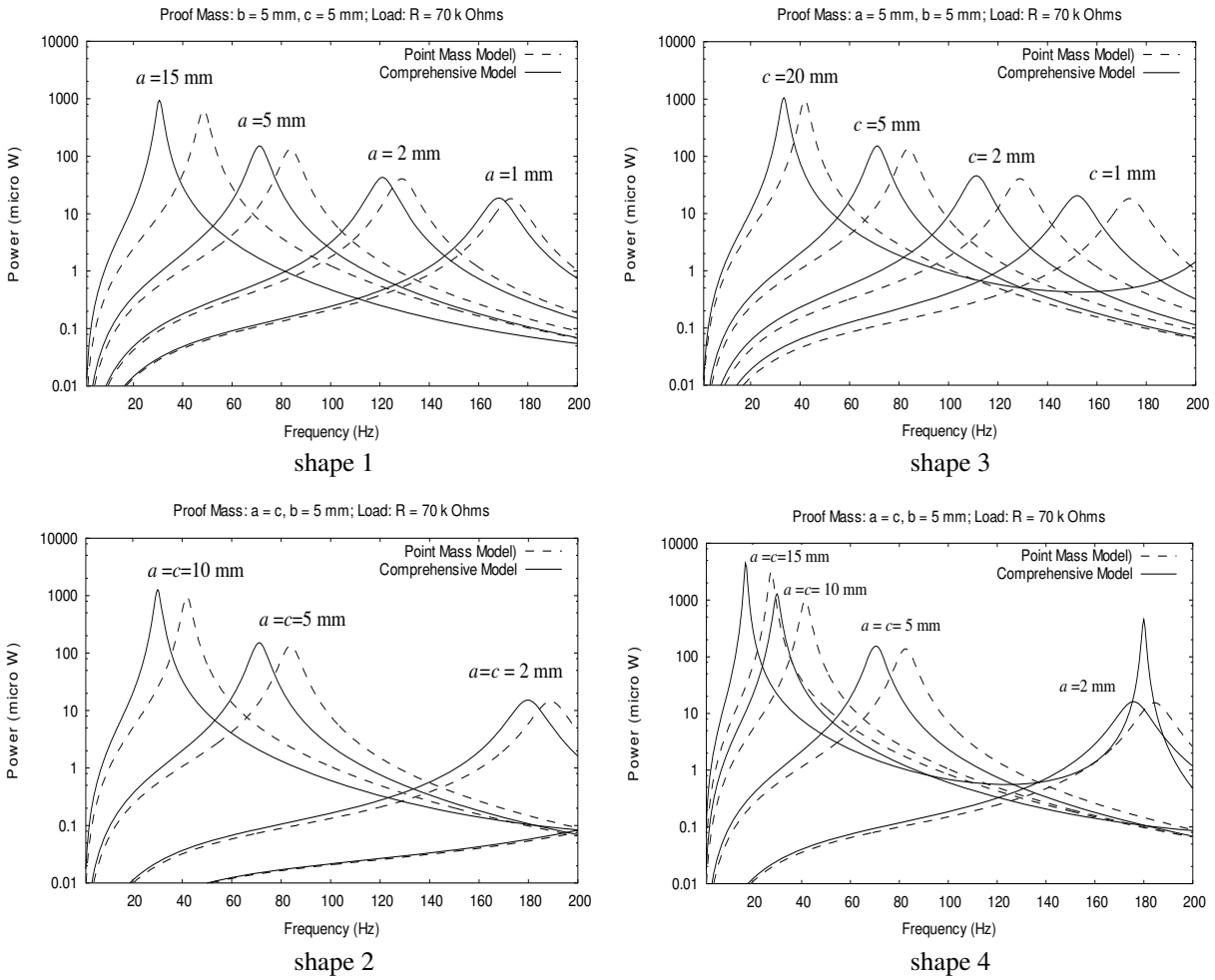

Figure 10. Effects of proof masses on output powers for $R = 70\,\mathrm{k}\Omega$.

Conclusions

A comprehensive model, along with a point mass model, is developed in this paper to simulate the mechanical motion and electrical power of piezoelectric bimorph energy harvesters. The mass moment of inertia and bending-axial stretching coupling effects due to a nonsymmetric proof mass configuration are considered in the comprehensive model. The simulation results from the point mass and comprehensive models are compared with independent data available in the literature for a series connection between the two PZT layers and newly obtained experimental data for a parallel connection. Excellent agreement was achieved between the theoretical predictions from the comprehensive model and the measurements for both sets of experiments. It is found that the point mass model produces significant errors for both the resonant frequencies and electrical powers. Sensitivity studies conducted using the comprehensive model show that the effects of mass, mass moment inertia, and mass center offset of a proof mass on the electrical power harvesting are significant and must all be taken into consideration in simulations.

References

[Anton and Sodano 2007] S. R. Anton and H. A. Sodano, "A review of power harvesting using piezoelectric materials: 2003–2006", *Smart Mater. Struct.* **16**:3 (2007), R1.

[Bathe 1995] K.-J. Bathe, *Finite element procedures*, 2nd ed., Prentice Hall, Englewood Cliffs, NJ, 1995.

[Dutoit et al. 2005] N. E. Dutoit, B. L. Wardle, and S.-G. Kim, "Design considerations for MEMS-scale piezoelectric mechanical vibration energy harvesters", *Integr. Ferroelectr.* **71**:1 (2005), 121–160.

[Erturk and Inman 2008a] A. Erturk and D. J. Inman, "Comment on 'Modeling and analysis of a bimorph piezoelectric cantilever beam for voltage generation"', *Smart Mater. Struct.* **17**:5 (2008), 058001.

[Erturk and Inman 2008b] A. Erturk and D. J. Inman, "Issues in mathematical modeling of piezoelectric energy harvesters", *Smart Mater. Struct.* **17**:6 (2008), 065016.

[Erturk and Inman 2009] A. Erturk and D. J. Inman, "An experimentally validated bimorph cantilever model for piezoelectric energy harvesting from base excitations", *Smart Mater. Struct.* **18**:2 (2009), 025009.

[Glynne-Jones et al. 2004] P. Glynne-Jones, M. J. Tudor, S. P. Beeby, and N. M. White, "An electromagnetic, vibration-powered generator for intelligent sensor systems", *Sens. Actuators A Phys.* **110**:1–3 (2004), 344–349.

[Liao and Sodano 2008] Y. Liao and H. A. Sodano, "Model of a single model energy harvester and properties for optimal power generation", *Smart Mater. Struct.* **17**:6 (2008), 065026.

[Mitcheson et al. 2004] P. D. Mitcheson, P. Miao, B. H. Stark, E. M. Yeatman, A. S. Holmes, and T. C. Green, "MEMS electrostatic micropower generator for low frequency operation", *Sens. Actuators A Phys.* **115**:2–3 (2004), 523–539.

[Roundy et al. 2004] S. Roundy, P. K. Wright, and J. M. Rabaey, *Energy scavenging for wireless sensor networks: with special focus on vibrations*, Kluwer Academic Publishers, Boston, 2004.

[Sodano et al. 2004] H. A. Sodano, G. Park, and D. J. Inman, "A review of power harvesting from vibration using piezoelectric materials", *Shock Vib. Digest* **36**:3 (2004), 197–205.

[Wang et al. 2007] F. Wang, G. J. Tang, and D. K. Li, "Accurate modeling of a piezoelectric composite beam", *Smart Mater. Struct.* **16**:5 (2007), 1595–1602.

[Yang 2006] J. Yang, *Analysis of piezoelectric devices*, World Scientific, Singapore, 2006.

[Yu and Cleghorn 2002] S. D. Yu and W. L. Cleghorn, "Dynamic instability analysis of high-speed flexible four-bar mechanisms", *Mech. Mach. Theory* **37**:11 (2002), 1261–1285.

Received 24 Jun 2009. Revised 26 Nov 2009. Accepted 26 Nov 2009.

SHUDONG YU: syu@ryerson.ca
Department of Mechanical and Industrial Engineering, Ryerson University, 350 Victoria Street, Toronto M5B 2K3, Canada

SIYUAN HE: s2he@ryerson.ca
Department of Mechanical and Industrial Engineering, Ryerson University, 350 Victoria Street, Toronto M5B 2K3, Canada

WEN LI: w3li@ryerson.ca
Department of Mechanical and Industrial Engineering, Ryerson University, 350 Victoria Street, Toronto M5B 2K3, Canada

JOURNAL OF MECHANICS OF MATERIALS AND STRUCTURES

http://www.jomms.org

Founded by Charles R. Steele and Marie-Louise Steele

See inside back cover or http://www.jomms.org for submission guidelines.

JoMMS (ISSN 1559-3959) is published in 10 issues a year. The subscription price for 2010 is US $/year for the electronic version, and $/year (+$ shipping outside the US) for print and electronic. Subscriptions, requests for back issues, and changes of address should be sent to Mathematical Sciences Publishers, Department of Mathematics, University of California, Berkeley, CA 94720–3840.

JoMMS peer-review and production is managed by EditFLOW™ from Mathematical Sciences Publishers.

PUBLISHED BY

mathematical sciences publishers

http://www.mathscipub.org

A NON-PROFIT CORPORATION

Typeset in LaTeX

Journal of Mechanics of Materials and Structures

Volume 5, No. 3 March 2010